Applied Magnetic Resonance (2019) 50:943–957
https://doi.org/10.1007/s00723-019-01122-y

Applied
Magnetic Resonance

ORIGINAL PAPER

Detection of Magnetosome-Like Structures in Eukaryotic Cells Using Nonlinear Longitudinal Response to *ac* Field

Vyacheslav A. Ryzhov[1] · Gabriele Multhoff[2] · Maxim A. Shevtsov[2,3,4,5]

Received: 23 January 2019 / Revised: 8 March 2019 / Published online: 20 March 2019

Abstract

Although magnetosomes have been discovered in bacteria since several decades, until today the question remains open whether such biomineralized structures do exist in eukaryotic cells. Herein, evidence was provided for the existence of magnetosome-like Fe-based structures in different viable eukaryotic cells by the registration of second harmonic of magnetization $M_2(H)$ of longitudinal nonlinear response to weak *ac* field. The behavior of the field hysteresis of the M_2 response from cells in suspension and/or in pellet indicated a multi-domain state of magnetosome-like structures in certain type of cells, and a single-domain state in other cell lines. The amounts of magnetosomes in cells range from $\leq 1 \div 2$ to $5 \div 8$ per cell. The presence of magnetosome-like structures was analyzed in normal tissue samples obtained from Wistar rats and C57/Bl6 mice. Additionally, the tumor tissue (orthotopic rat C6 glioma and mouse GL261 glioma) were assessed for magnetosomes. Detected magnetosomes in certain tissues (i.e., brain, heart, lungs) matched to a single-domain magnetite nanoparticle, whereas in other organs they exhibited characteristics attributable to a multi-domain state, better corresponding to Fe(0) composition of their magnetic cores. Subsequent studies are necessary to elucidate the role of the Fe-based magnetosome-like structures in the biology and physiology of eukaryotic cells.

1 Introduction

Magnetosomes are unique organelles which are predominantly found in prokaryotes. Functionally, they are responsible for magnetotaxis in prokaryotes [1, 2]. Magnetosomes consist of magnetic mineral crystals, containing either magnetite (Fe_3O_4) or greigite (Fe_3S_4), which are surrounded by a bilayer membrane composed predominantly by phospholipids and a number of proteins that are not present in the cytosol or in the outer membranes (OMs) [3, 4]. Magnetotaxis is

✉ Maxim A. Shevtsov
maxim.shevtsov@tum.de

Extended author information available on the last page of the article

responsible for an optimal positioning of bacteria in vertical chemical concentration gradients by reducing the three-dimensional search problem to a single dimension [5]. Although magnetosomes have been discovered in bacteria since several decades [2, 6], the question about the existence of such biomineralized structures in eukaryotic cells has not been answered.

Magnetotaxis which is achieved by the presence of lipid-bound magnetosomes in the magnetotactic bacteria (MTB) aids bacteria to identify optimal growth conditions [7, 8]. Although numerous studies clearly demonstrate an influence of low-frequency electromagnetic fields (LF-EMFs) in biological systems [9–13], studies in eukaryotic cell systems mostly remain phenomenological without mechanistic insights. Although ferromagnetism has been described for the magnetotaxis of bacteria and for the navigation of animals (e.g., birds, turtles) [14, 15], it remains to be determined whether similar structures are present in eukaryotic somatic cells that could explain the phenomenon of magnetoreception [9] which might influence cell development and differentiation. Presumably the cell-sensing mechanism lies in the existence of magnetosome-like structures that could respond to static and/or oscillating magnetic fields.

A previous biodistribution study of a targeted delivery of functionalized superparamagnetic iron oxide nanoparticles (SPIONs) in tumor-bearing rats resulted in the discovery of a small amount of intrinsic magnetic nanoparticles (MNPs) in tissues such as heart, skin, muscle, lungs, and tumors of control animals that had not been injected with SPIONs [16–18]. With respect to this finding, the possible presence of magnetosome-like structures was assessed in cell suspensions of viable normal cells [i.e., chondrocytes, osteocytes, and mesenchymal stem cells (MSCs), etc.] as well as in normal tissues such as heart, skin, brain, and tumor tissues (i.e., rat C6 glioma and mouse GL261 glioma). The very low concentrations of the detected magnetosome-like structures inside eukaryotic cells exclude the use of electron microscopy to identify them. However, highly sensitive nonlinear longitudinal responses to a weak *ac* magnetic field with registration of second harmonic magnetization M_2 (NLR-M_2) could be employed for the analysis of these magnetosomes in vitro. This approach was employed earlier for the investigation of the biodistribution of SPIONs in tumor-bearing rats and allowed to reveal intrinsic MNPs in tissues of control animals [16–18]. The high sensitivity of this approach is provided, on the one hand, by registration of responses on a frequency that differs from the frequency of *ac* field which affects the sample during the study. This allows the separation of the signal of a sample from a high-level voltage-excited field at the input of the receiver using radio-frequency (RF) methods (see details below), and to register the former against the background of the thermal noise of the receiver [19–21]. While in *ac* susceptibility measurements or ESR studies a signal from a sample represents a small change of *ac* field $h(t)$ level and registers against the background of the amplitude and frequency noise of RF generator that hinders to increase $h(t)$ for enhancement of the signal. On the other hand, the use of nonlinear responses allows the enhancement of signals from MNPs in comparison with ambient paramagnetic species with a large nonlinearity on MNP magnetization $M(H)$ in a weak field H. The latter is followed by the presence of a specific extremum at a weak H in $M_2(H)$ dependence

[22–25]. It is registered against very weak M_2-responses from paramagnetic species [since their $M(H)$ nonlinearity is negligible in the weak field H] with the linear dependency on H. This provides large suppression of the contribution to the signal from ambient organelles and components of eukaryotic cells containing species with paramagnetic properties. In measurements of low frequencies *ac* susceptibility (in this case the latter is close to the static one), a contribution from paramagnetic species will dominate due to their large amount making it very difficult to extract the MNP response. In magnetic resonance measurements MNPs reveal wide spectra due to effective relaxation and inhomogeneous broadening because of the arbitrary orientation of their anisotropy axes. Therefore, the contribution from small amounts of MNPs is not detectable against the background of narrow and intensive ESR signals from paramagnetic species as it was previously found in carbon-based porous nanomaterials [25]. In measurements of static magnetization by SQUID magnetometer an additional problem appears since this method is sensitive also to the diamagnetic contribution of samples as well as of the cavity.

2 Methods

2.1 *NLR-M_2* Measurements

MNPs possess a large magnetic moment, therefore, magnetization $M(H)$ of MNP's ensemble exhibits saturation in a weak *dc* field H. As a result the ensemble response to the ac field $h(t)$ in the presence of the parallel to it *dc* field H reveals distortions relative to the sinosoidal *ac* field. The latter are non-symmetric for positive and negative signs of $h(t)$ as it is schematically shown in the left panel of Fig. 1. Therefore, mainly the even harmonics of fundamental frequency f will be generated in a sample during the study, and only the largest second harmonic, M_2, is registered.

The main features of the experimental setup, providing the high sensitivity of this approach can be briefly summarized as follows: (1) the employment of two-mode (f, $2f$) resonant sensor (2-mode sensor) providing: (1) the creation of *ac* field of frequency $f = 15.7$ MHz and amplitude h up to 50 Oe in radio-frequency (RF) inductance coil L (with sample under study inside) included in both (f), and ($2f$) modes; (2) effective registration of a sample $M_2(H)$ response, inducing $2f$-voltage in RF coil L, with help of mode ($2f$); (2) deep suppression of the $2f$-voltage from f-generator by low-frequency filter, including the input mode (f); (3) deep suppression of f-voltage from the output of mode ($2f$) by high-frequency filter, including at the input of the $2f$-receiver; (4) the use of in 2-mode sensor elements and materials, which are not produced spurious $2f$-signal. Under these conditions it is possible to register the M_2 signal of a sample against the background of thermal noise of the receiver [19–21]. Note, Q_2-factor of $2f$-mode is about 200 that provides increase of setup sensitivity by $\sim Q_2^{1/2}$ in comparison with non-resonant registration of $\chi(f)$ in *ac* susceptibility measurements.

At M_2 measurements both M_2 components, $\mathrm{Re}M_2(H)$ and $\mathrm{Im}M_2(H)$, are simultaneously recorded as functions of H synchronously with its scan. For detecting

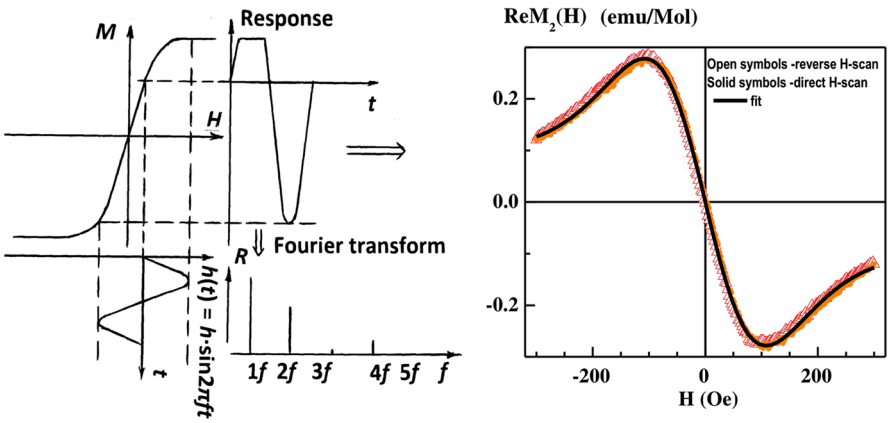

Fig. 1 Origin of second harmonic of magnetization $M_2(2f)$ of nonlinear response to a weak *ac* field $h(2\pi ft)$ in parallel to its *dc* field H from system of magnetic nanoparticles (MNP)—left panel. Right panel presents a typical ReM_2 response vs steady field H from ensemble of dextran-coated Fe_3O_4 MNPs (often used in medicine application) in water suspension with effective Fe concentration 2×10^{-5} Mol/L at $T=300$ K. Average size of magnetite core is ~ 10 nm. A weak dynamical field hysteresis (difference between curves registered at direct and reverse H-scan) can be seen in Re$M_2(H)$ at used $F_{scan}=8$ Hz, which disappears at $F_{scan}=1.32$ Hz (not shown). The fit of average curve was performed by Re$M_2(H) \propto \partial^2 L(H)/\partial H^2$, here $L(H)$ is Langevin function. The found value of NP average moment is $\mu_{aver} \approx 5.96\cdot10^4$ μ_B. Very small linear contribution from low-molecular paramagnetic fraction was taken into account at fitting

the field hysteresis, H was linearly scanned symmetrically relative to the point $H=0$ with frequency F_{sc} without constant bias field H_0. The amplitude of H-scan was 300 Oe and its frequency, F_{sc}, could be varied in the range 8 Hz $\geq F_{sc} \geq 10^{-2}$ Hz. Sample temperature was stabilized by flow thermostat, using evaporated N_2. Different magnetics can be investigated by this technique, including systems with strong electronic correlations ([22–25] and Refs. therein), its integral sensitivity of M_2 registration being about 10^{-10} emu.

Usually the condition $M_2 \propto h^2$ is fulfilled in the experiment, and allows the application of the perturbation theory. In this case the susceptibility of second order $\chi_2=M_2/h^2$ can be introduced. For the ensemble of MNPs in superparamagnetic (SPM) regime when average anisotropy energy of MNP is less of energy of thermal fluctuations kT (k is the Boltzmann constant and T is temperature) $\chi_2(H, T)$ is described by the simple expression [22–25]:

$$\chi_2(\omega) = \frac{\Gamma}{-2i\omega+\Gamma}\chi^{(2)} - i\omega\frac{(\partial/\partial\omega_0)\Gamma}{(-2i\omega+\Gamma)(-i\omega+\Gamma)}\chi^{(1)}; \quad (1)$$

Here $\chi^{(1)}=\partial M(H)/\partial H$, $\chi^{(2)}=(1/2)\ \partial^2 M(H)/\partial H^2$, Γ is a magnetic relaxation rate, $\omega=2\pi f$, $\omega_0=g\mu_B H/\hbar$ is the Larmor frequency and μ_B is the Bohr magneton. The first term in (1) arises due to a nonlinearity of magnetization curve $M(H)$, it exhibits a static limit and provides the main contribution to the real part of the response,

Re$M_2(H)$, which is proportional to concentration of MNPs. The second one is due to influence of external magnetic field on relaxation process; it has no static limit and provides the main contribution to the imaginary part of the response, Im$M_2(H)$, which exhibits an opposite sign relative to ReM_2. Thus, as it is partly seen from Eq. (1), M_2-response from MNP ensemble exhibits three peculiarities that can be considered as "finger print" of such systems [16, 22–25]: (1) the presence of extremes in a weak steady magnetic field in both phase components due to strong nonlinearity of $M(H)$; (2) opposite signs of signals in phase components of response (negative in Re$M_2(H)$ and positive in Im$M_2(H)$ in $H>0$ region) owing to different physical reasons creating the contribution to them in accordance with Eq. (1); (3) the presence of field hysteresis that reveals dynamical character in case of single-domain MNPs (in our case it is changed at varying frequency of H-scan). The first and third features can be seen in Re$M_2(H)$ response of dextran-coated single-domain Fe_3O_4 MNPs (often used in medicine application) in water suspension displayed in right panel of Fig. 1. The effective Fe concentration was 2×10^{-5} Mol/L, and average size of magnetic core ~ 10 nm. MNPs are close to superparamagnetic (SPM) regime near room temperature that is indicated by small-field hysteresis. In this case, their magnetization can be described by the classical Langevin function $M(H)=mN\cdot L(mH/kT)=mN\cdot(\mathrm{cth}(mH/kT)-kT/mH)$ (m is an average magnetic moment of MNP, N is the number of MNPs in sample). The fit of Re$M_2(H)$ by $\partial^2M(H)/\partial H^2$ is presented together with experimental curves. It allows us to estimate an average moment of MNPs, $m_{\mathrm{aver}}\approx6\times10^4\ \mu_B$. The complete description of both Re$M_2(H)$ and Im$M_2(H)$ from an ensemble of the single-domain MNPs in SPM regime can be obtained from analysis of $M_2(H, T)$ data with employment of Gilbert–Landau–Lifshits equation formalism [23] and allows one to determine their static and dynamic parameters as well as a distribution of magnetic moment values in ensemble. However, this issue is out of the scope of this paper.

In case of single-domain non-interacting MNPs, the presence of field hysteresis evidences a deviation from SPM regime provided by the magnetic anisotropy. The latter includes contributions of magneto-crystalline, form and surface anisotropy of MNPs [24, 26]. In widely common case of the simple uniaxial anisotropy the rate of relaxation of MNP ensemble is given by $\Gamma=1/\tau=f_0\exp(-E_a/kT)$ (without taking into account the effect of field on the relaxation processes) [26]. Here anisotropy energy $E_a=KV$, K is anisotropy constant, V is an average volume of a particle and the frequency f_0 is of the order of $10^9\ \mathrm{s}^{-1}$. The probability that the magnetization remains in its original position during time t after switching off the external field can be written as $P(t)=\exp(-t/\tau)$, that gives for retentivity $M_{\mathrm{ret}}(t)/M_0=\exp(-t/\tau)$. Thus, if the registration time is less than τ, the M_{ret} and H-hysteresis will be detected. In our case of the periodic H-scan, the dynamical H-hysteresis will be observed in Re$M_2(H)$, when a period of H-scan $F_{\mathrm{sc}}^{-1}\le\tau=\Gamma^{-1}$. When the time of measurements is equal to relaxation time $\tau^*=F_{\mathrm{sc}}^{-1}=\tau$, the blocking temperature T_B can be introduced, above which the behavior of the system will be superparamagnetic [26]:

$$T_B=KV/\left[k\cdot\ln\left(f_0/F_{\mathrm{sc}}\right)\right]. \tag{2}$$

Note, as Eq. (2) shows, T_B depends on experimental conditions, namely, on time F_{sc}^{-1} that system has for the thermal equilibrium before the moment reversal. So

varying F_{sc} permits one to alter T_B and H-hysteresis of M_2 response of the single-domain MNPs. The example of dynamic H-hysteresis can be seen in the right panel of Fig. 1, where the signal of dextran-coated single-domain magnetite MNPs close to superparamagnetic (SPM) regime is displayed. The field hysteresis disappears at $F_{sc} = 1.32$ Hz (not shown). In multi-domain state of MNPs the hysteresis should be practically invariable since it is due to pinning of magnetic moment on structure heterogeneities. In this case the magnetization reversal is determined by movement of domain boundaries instead of MNP moment rotation, and the former is much faster than F_{sc}^{-1} [26]. Thus, the regime of magnetic behavior of MNPs and its possible transformation under effect of environment can be controlled by a simple way on a presence of H-hysteresis in their M_2-response. The latter can be characterized by ReM_2 "coercivity", H_{C2} shown in Fig. 2a, which is found from the condition Re$M_2(H_{C2}) = 0$. Its dependence on F_{sc} and temperature allows one to discriminate single-/multi-domain states of MNPs and to determine T_B [24].

2.2 Cells

Rat C6 glioma and mouse GL261 glioma cell lines were grown at 37 °C in RPMI-1640 cell medium supplemented with 10% fetal bovine serum (FBS),

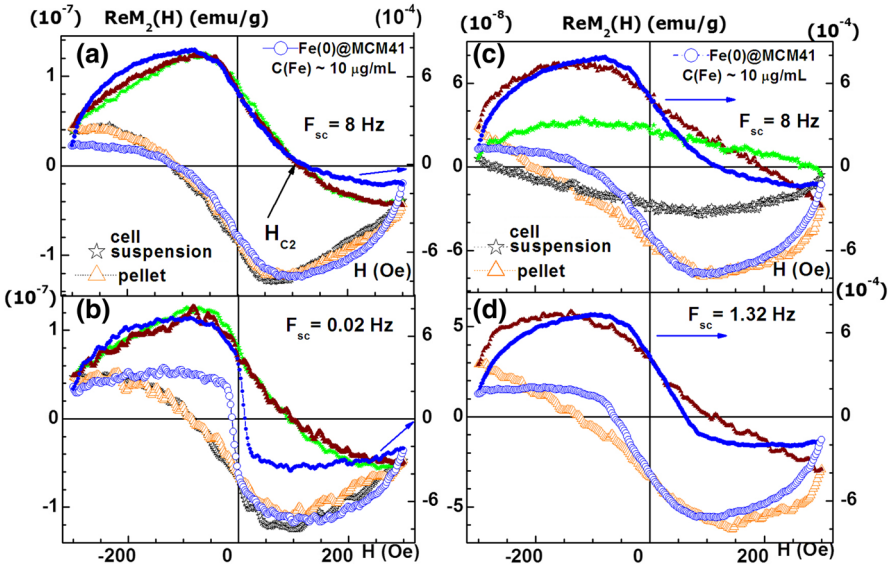

Fig. 2 Re$M_2(H)$ signals from mesenchymal stem cells (MSCs) of synovial tissue with chondrocytes (MSC + CC) in suspension and sediment are presented at some frequencies of H-scan: (1) $F_{sc} = 8$ Hz (panel **a**); (2) $F_{sc} = 0.02$ Hz (panel **b**). Re$M_2(H)$ signals from MSCs of marrow induced in osteocyte cells (MSC_OC) in suspension and sediment are displayed as well at some frequencies of H-scan: (1) $F_{sc} = 8$ Hz (panel **c**); (2) $F_{sc} = 1.32$ Hz, without signal from sediment (panel **b**). Besides, Re$M_2(H)$ signals from suspension of Fe(0)@MCM41 MNPs (with effective concentration of Fe, C(Fe) ≈ 0.1 mg/mL) are shown also in each panel at corresponding F_{sc}. ReM_2 "coercivity", H_{C2}, determined from the condition Re$M_2(H_{C2}) = 0$ is presented in panel **a**

2 mM L-glutamine and antibiotics (100 units/mL Penicillin G and 100 µg/mL Streptomycin). Cell lines were regularly tested negative for mycoplasma contamination. Cells were passaged twice a week and single-cell suspensions were derived by short-term (less than 1 min) treatment with 0.25% (w/v) Trypsin-0.53 mM EDTA.

2.3 Mesenchymal Stem Cells

Mesenchymal stem cells (MSCs) were obtained from the bone marrow of New Zealand rabbits by flushing the femur with αMEM medium (Lonza, Allendale, NJ, USA) supplemented with 10% fetal bovine serum (FBS) (HyClone, Utah, USA), 100 U/mL penicillin (Sigma-Aldrich, WGK Germany) and 100 µg/mL streptomycin (Sigma-Aldrich, WGK Germany). The marrow plug suspension was dispersed by pipetting, filtered through a 70 µm mesh nylon filter (Becton–Dickinson Biosciences, Bedford, MA, USA) and centrifuged at 400×*g* for 5 min. The pellet was resuspended in Red Blood Cell Lysis Solution (0.154 M NH_4Cl, 10 mM $KHCO_3$ and 0.1 mM EDTA) (Panreac, Barcelona, Spain) for 5 min and centrifuged at 400×*g* for 5 min. Cells (1×10^7) were seeded into 100 mm culture dishes (Nunc; Thermo Fisher Scientific, Waltham, MA, USA) and incubated at 37 °C and humidified with 5% CO_2.

2.4 Isolation of Primary Chondrocytes

Rabbit cartilage obtained from articular surfaces was minced and sequentially digested by the following Sigma-Aldrich enzymes, 0.05% hyaluronidase, 0.25% trypsin and 0.4% collagenase to harvest primary chondrocytes for monolayer culture. The isolated cells were washed and suspended in DMEM-F12 complemented with 15% FBS (GIBCO/Life Technology, NY, USA) and 1.0% penicillin–streptomycin solution. Prepared primary chondrocytes were seeded in 25-cm^2 flasks with 8×10^5/mL cells and cultured in DMEM-F12 medium till 80% confluence followed.

2.5 Primary Osteocytes

Purified osteocyte and primary osteoblasts were derived from both parietal bones. Briefly, rabbit's parietal bones of the calvaria and tibiotarsal bones were cleared of the surrounding soft tissue and periostea. Medullary cavities were flushed with a Dulbecco phosphate-buffered saline (Invitrogen, Paisley, UK), Three sequential digestions of bone segments with 1 mg/mL collagenase type 1 (*Clostridium histolyticum*, Sigma, Dorset, UK) in PBS followed by 4 mM ethylenediaminetetraacetic acid (Sigma) in PBS. Digestion was stopped by incubation with 10% FBS in a Hank-balanced salt solution (HBSS) (Invitrogen), and each of these three consecutive fractions were centrifuged (800*g*, 4 °C for 5 min) and then resuspended in heat-inactivated chicken serum in an HBSS on ice. A single-cell suspension was resuspended in PBS containing 4 mM ethylenediaminetetraacetic acid and 0.5% bovine serum albumin (BSA; Fraction V, Sigma) (PEB) to produce a mixed bone-derived cell population. Bone-derived cells were cultured in Dulbecco Modified Eagle Medium

minus phenol red, 5% FBS, 2 mM L-glutamine, 50 µg/mL gentamicin (Invitrogen); 50 µg/mL L-ascorbic acid; 5.6 mM glucose (Sigma).

2.6 Animals

Male Wistar rats weighing 300–320 g and C57Bl/6 mice weighing 20–25 g were purchased in animal nursery "Rappolovo" RAMN (St. Petersburg, Russia). All animal experiments have been approved by the local ethical committee of First Pavlov State Medical University of St. Petersburg (St. Petersburg, Russia) and were in accordance with institutional guidelines for the welfare of animals. Animals were anesthetized before mounting in stereotactic frame (David Kopf Instruments, Tujunda, CA) with 10 mg "Zoletyl-100" (Vibrac sante Animale, France) and 0.2 mL 2% Rometar (Bioveta, Czech Republic) intraperitoneally. C6 cell suspension (1×10^6 cells/mL) in 10 µL was injected into the *nucl.caudatus dexter* of Wistar rats. GL261 cell suspension (1×10^6 cells/mL) in 2 µL was injected intracranially in C57Bl/6 mice.

3 Results and Discussion

We have performed NLR-M_2 investigations of suspensions of several cell cultures: (1) mesenchymal stem cells (MSCs) of synovial tissue with chondrocytes; (2) MSCs of newborn rabbit; (3) chondrocytes (CC); (4) MSCs of bone marrow of newborn rabbit; (5) MSCs of bone marrow of newborn rabbit induced to form osteocytes; (6) human osteosarcoma cells (HOS). Since precipitated cells can be considered as some model of a tissue the comparative measurements of samples with suspensions without pellet and precipitated cells were carried out to understand if the cell contacts affect parameters of M_2 response in comparison with the single-cell suspension. Part of these results is presented in Figs. 2, 3. All the experiments were performed at room temperature.

All the samples exhibit $M_2(H)$ signals revealing extremum in a weak field, opposite signs of signals in ReM_2 and ImM_2 components (the latter is basically not shown) and H-hysteresis, which was appreciably larger than that of single-domain Fe_3O_4 MNPs close to SPM regime presented in Fig. 1. This suggests the presence of magnesome-like structures, including magnetic (probably Fe-based) core in studied cells similar to that in prokaryotes [1, 2]. Note, as a rule, the field hysteresis of Re$M_2(H)$ signal from suspensions of studied cell cultures was larger or equal to this of samples with precipitated cells assuming some potential effects of cell contacts on the response parameters (see Figs. 2, 3). The presence of considerable H-hysteresis in the $M_2(H)$ response of magnetosome-like particles evidences blocking regimes or multi-domain state of their magnetic core. To clarify this issue we have studied the dependency of the $M_2(H)$ response on the frequencies of H-scan, F_{sc}.

Figure 2 presents the detected Re$M_2(H)$-phase component dependencies of the response of MSCs of synovial tissue with chondrocytes (MSC + CC), see panels (a, b), and of MSCs of marrow induced in osteocytes (MSC_OC) (panels c, d) in

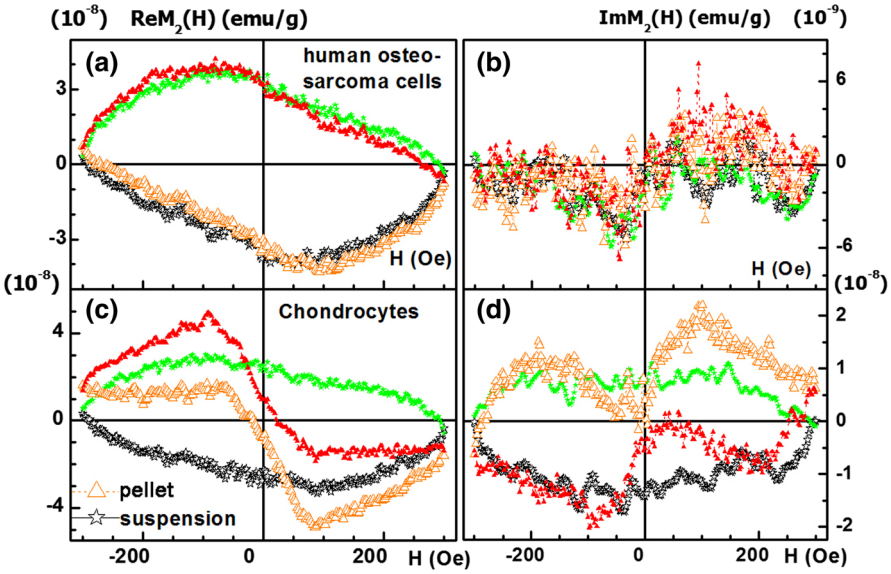

Fig. 3 Phase components of $M_2(H)$ response from human osteosarcoma cells and chondrocytes in suspension and in sediment

suspension or as a pellet at some frequencies of H-scan. As noted, the MSC + CC suspension, providing the maximal M_2 signal among the assessed cell suspensions, does not reveal any noticeable difference in M_2 parameters for suspension and pelleted samples while in MSC_OC cell cultures a larger hysteresis was observed in case of single-cell suspensions. In all panels the Re$M_2(H)$ curves are displayed from colloidal solution of the well-characterized earlier-used single-domain Fe(0)@MCM41 MNPs, registered at corresponding F_{sc} [17] with an effective Fe concentration of C(Fe) ≈ 0.01 mg/mL. The shape of Re$M_2(H)$ hysteretic curves of the latter is close to that of cell suspensions at $F_{sc} = 8$ Hz, (see panels a, c) assuming the Fe nature of the magnetic cores of magnetosome-like structures, which generate the M_2 response of the cell samples.

As shown in the Fig. 2a, b, decreasing of the F_{sc} is followed by a substantial decrease of H-hysteresis in signals of the single-domain Fe(0)@MCM41 MNPs that are in the blocking regime, while the latter is practically absent in the response of MSC + CC samples both in suspension and in pellet. This is indicative for a mainly multi-domain status of magnetosome magnetic cores in this sample. These multi-domain magnetosome-like patterns of eukaryotic cells are different from chainlike single-domain magnetosomes described for bacteria and protists [27, 28]. At the same time, the response of the MSC_OC cells reveals a decreasing H-hysteresis similar to that of Fe(0)@MCM41 MNPs (at F_{sc} decreasing the positions of ReM_2 "coercive force", H_{C2}, move to lower field for both samples and only their relative positions approximately conserved), at least, for pelleted MSC_OC cells, see Fig. 2c, d. This implies some contribution of the

magnetic moment rotation in moment reversal of "magnetosome" magnetic cores that is indicative for only a few magnetic domains.

The assumption of the Fe(0) nature of magnetic cores in magnetosome-like structures allows one to estimate Fe(0) concentration inside according to the amplitude of the latter compared to that of the Fe(0)@MCM41 (Fig. 2a, c). This results in: (1) $C(Fe) \sim (1.2\times10^{-7}/7.9\times10^{-4})\cdot[C(Fe)=0.01$ mg/mL$] \approx 1.5\times10^{-3}$ μg/mL = 1.5 ng/mL for MSC + CC sample; and (2) $C(Fe) \sim (7.4\times10^{-8}/7.9\times10^{-4})\cdot$ [C(Fe) = 0.01 mg/mL] $\approx 9\times10^{-4}$ μg/mL = 0.9 ng/mL for MSC_CO one. The volume of the samples was always 0.5 mL and the concentration of cells in suspension was $\sim 10^5$ cells/mL which allows an estimation of the Fe content per cell of $\sim 1.5\times10^{-5}$ ng and $\sim 0.9\times10^{-5}$ ng for considered samples accordingly. Transforming these quantities in moles of Fe(0) we obtain $\sim 2.7\times10^{-16}$ mol(Fe)/cell and $\sim 1.6\times10^{-16}$ mol(Fe)/cell, respectively. The latter corresponds to $\sim 1.6\times10^{8}$ (Fe atoms)/cell and $\sim 9.6\times10^{7}$ (Fe)/cell accordingly.

The critical diameter of single-domain Fe nanoparticles is estimated as ~ 20 nm [29]. Therefore, the diameter of of multi-domain magnetosome-like structures of MSC + CC and MSC_OC is not less than the double-critical size of the Fe magnetic core of ~ 40 nm. Approximately 2×10^7 Fe-atoms should correspond to this minimal size of the magnetic core. The latter estimation matches to the maximum of $\sim 5 \div 8$ "magnetosomes" per cell (for MSC + CC and MSC_OC cells). M_2 response from other cell lines is at least $3 \div 5$-times less indicating the presence of $\leq 1 \div 2$ magnetosomes per cell. This fact hampers the application of electron microscopy for the magnetosomes' identification in the cells.

Figure 3 displays the results of NLR-M_2 measurements carried out on human osteosarcoma (HOS) cells and chondrocytes in suspension and precipitated samples. As shown in panels (a), (b) the response of HOS cells is practically independent of their aggregate state (single-cell suspension or precipitated sample) similar to that of MSC + CC cells, although the "magnitosome" amount in them ($\propto$ amplitude of their signal) is drastically lower. At the same time the aggregate state of other cell cultures, chondrocytes, strikingly affects on H-hysteresis of their M_2 response, as it can be seen in Fig. 3c, d. Therefore, Fig. 3 supports the above-postulated generalizations.

Biodistribution studies of control tissues of glioma-bearing rats (tumor, heart, etc.) without MNP revealed hysteretic $M_2(H)$ signals in NLR-M_2 experiments implying the presence of internal MNPs in them [16–18]. In this work we performed similar measurements in probes of rats with C6 glioma and mice with GL261 glioma to confirm the presence of the magnetosome-like structures in tissues of several organs and in tumor cells, to compare the data with those of cultured cells. The results are displayed in Fig. 4.

The comparison of $\mathrm{Re}M_2(H)$ amplitudes in panels (a), (b) of Fig. 4 shows increased amounts of magnetosome-like structures in mouse glioma. Besides, a weak "coercivity" signal detected in rat glioma (Fig. 4a) suggests the state of its magnetosome-like magnetic cores close to single-domain one in the blocking regime. While in mouse glioma, the multi-domain state of the latter is definitely realized since its $\mathrm{Re}M_2(H)$ "coercivity" does not change at increasing time of measurement (during one cycle of H-scan) from 0.125 s ($F_{sc} = 8$ Hz) up to 4 s ($F_{sc} = 0.25$ Hz), see panel (b). Indeed, in case of single-domain MNPs in blocking regime, H_{C2} should decrease at a reduction of F_{sc} due to decrease of the blocking

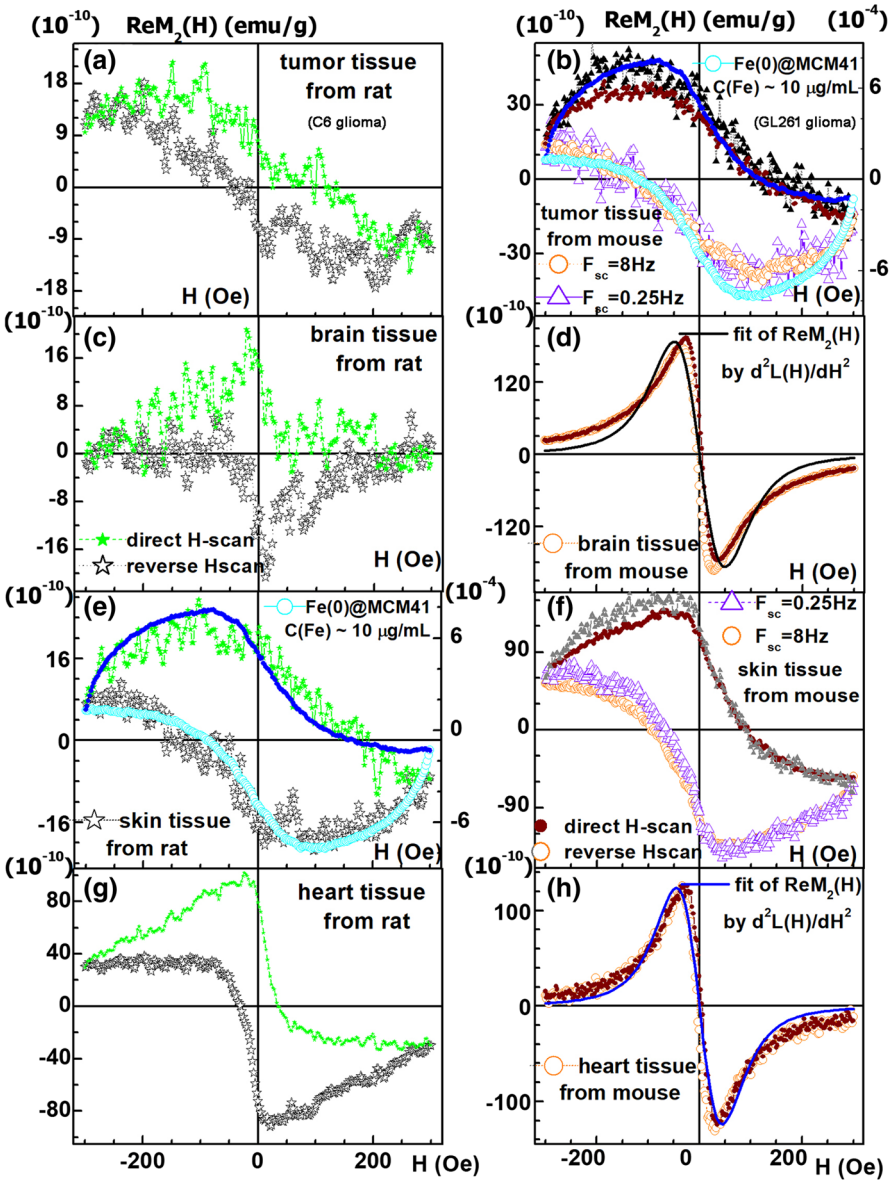

Fig. 4 Re$M_2(H)$ signals from C6 glioma and normal tissues (brain, skin, heart) of the rat (left column, panels **a**, **c**, **e**, **g**) and GL261 glioma as well as normal tissues (brain, skin, heart) of the mouse (right column, panels **b**, **d**, **f**, **h**). In all the panels the presented signals were obtained at $F_{sc}=8$ Hz while in panels (**b**) and (**f**) the signal from tumor and skin tissues of mouse recorded at $F_{sc}=0.25$ Hz is shown as well. In panels (**b**, **e**) the Re$M_2(H)$ signals from suspension of Fe(0)@MCM41 MNPs [with effective concentration of Fe C(Fe)$\approx$0.1 mg/mL] are displayed for comparison. Panels (**d**, **h**) present also the results of Re$M_2(H)$ fit by $\partial^2 L(H)/\partial H^2$, here $L(H)$ is the Langevin function

temperature (in agreement with Eq. 1) similar to this for Fe(0)@MCM41 MNPs (see Fig. 2b). The form of the Re$M_2(H)$ response from mouse tumors is similar to that of the Fe(0)@CMC41 MNPs, implying close to Fe(0) composition of its magnetosome-like magnetic core. Similar features are found in the Re$M_2(H)$ response of mouse skin tissue [panel (f)], assuming the same state of magnetic core in it. The close or even larger value of H_{C2} in signals of the rat skin tissue (Fig. 4e) is indicative for similarities in their magnetosomes-like structures although, their concentrations are smaller which is in agreement with a lower signal amplitude.

Signals from mouse brain sample [i.e., Re$M_2(H)$ responses] (Fig. 4d) definitely correspond to that of single-domain MNPs close to the SPM regime. Indeed, the decreasing of F_{sc} down to 0.25 Hz leads to a collapse of the ReM_2 field hysteresis (data not shown). The best fit of Re$M_2(H)$ curve by corresponding functions obtained from the Langevin is shown in Fig. 4d with a value of MNP average moment of $\mu_{aver} \approx 1.24 \times 10^5\ \mu_B$. This value is larger than $6 \times 10^4\ \mu_B$ obtained from the same best fit of Re$M_2(H)$ response of dextran-coated Fe_3O_4 MNPs with an average diameter of ~ 10 nm while the "coercivities" and forms of both signals are similar (Fig. 1). These results argue for a magnetite core in mouse brain magnetosome-like structures with about two times larger volumes of their magnetic cores ($d_{aver} \sim 13$ nm). The description of the signal by fitting curves is not suitable since the considerable affect of magnetic field on relaxation processes was not taken into account for the fitting. This is evidenced by the presence of the Im$M_2(H)$ component of the weakly hysteretic signal which is comparable with the Re$M_2(H)$ amplitude and an opposite (positive in $H > 0$ region) sign which is due to this affect [23, 24]. The signal from the rat brain is almost, by an order of magnitude, smaller and exhibits larger H-hysteresis (H_{C2}) whereas the position of its extremum is in a similar weak field H. This indicates the smaller amount of magnetosome-like structures in rat brain and does not allow to assume a magnetite nature of magnetosome-like cores in rat brain. However, drastically larger magnetic anisotropy is observed in rats compared to mice. The latter should be accompanied by blocking regime of their behavior leading to larger H-hysteresis in Re$M_2(H)$ in agreement with the data.

Comparative analysis of the M_2 responses from normal brain and glioma tissues could indicate a plausible transformation of magnetosome-like magnetic core state from magnetite to Fe(0) in tumor cells.

The features of Re$M_2(H)$ signals from heart tissue of the control mouse are similar to those of brain (Fig. 4h) and indicate the plausible magnetite composition of magnetosome-like magnetic cores in it which are close to SPM regime behavior. The fit of response by the same function obtained from Langevin includes the slightly larger value of the MNP average moment $\mu_{aver} \approx 1.38 \times 10^5\ \mu_B$, which is also presented in this Fig. 4. The observed discrepancy of experimental signal and fitting curve is explained again by the presence of the non-considered contribution to the response from the effects of the external magnetic field on relaxation processes [23, 24]. The more hysteretic Re$M_2(H)$ signal from heart tissue of the control rat exhibits a comparable amplitude with extremum position in a weak field close to that of the mouse response. This shows the presence of a comparable amount of magnetosome-like structures with magnetite core in heart tissues of both rodents but

their arrangement in the rat is accompanied by a larger magnetic anisotropy that is followed by a crossover to the blocking regime.

Noteworthy, magnetosome $M_2(H)$ response from mouse organs which are well oxygenated (brain, heart, lungs) matches to that of single-domain magnetite nanoparticles, whereas magnetosomes of other organs with a lower oxygen supply reveal hysteretic signals that correspond better to a Fe(0) multi-domain magnetic core.

One could suggest various physiological functions of the detected magnetic structures in somatic cells including magnetotaxis, scavenging the reactive oxygen species and exhibiting peroxidase-like activities [30], or homing of the cells to a certain microenvironment. The described magnetosome-like structures in eukaryotic cells represent most probably the Fe-based nanostructures, whose magnetic state (single-domain, multi-domain) depends on the type of cells and their aggregate state. Subsequent studies are necessary to elucidate the role of the Fe-based magnetosome-like structures in the biology and physiology of eukaryotic cells, and to compare carefully their organization with linear chain(s) of biologically produced nano-sized single-domain magnetite crystals in prokaryotes. We anticipate that our data provide only a first hint for more sophisticated in vitro analysis of the role of magnetosome-like structures in the magnetotaxis of eukaryotic cells.

4 Conclusion

In the current study the investigations of magnetic nonlinear response to a weak *ac* field of eukaryotic cells were performed with the employment of the highly sensitive method of NLR-M_2 measurements. The use of nonlinear responses allows the enhancement of signals from MNPs in comparison with ambient paramagnetic species owing to large nonlinearity on their magnetization $M(H)$ in a weak field H. All studied samples reveal $M_2(H)$ responses characteristic for MNPs, signal of maximal amplitude being lowest in mesenchymal stem cells of synovial tissue and highest in chondrocytes. The observed signals exhibit the features of MNPs $M_2(H)$ response and can be attributed to the magnetosome-like structures with Fe-based magnetic cores existing in the analyzed eukaryotic cells. The comparative analysis of the obtained $M_2(H)$ dependencies of the cell samples and those of single-domain Fe(0)@MCM41 MNPs are indicative for the multi-domain magnetic state of magnetic cores in magnetosome-like structures of eukaryotic cells. None of the cell samples showed superparamagnetic regime of behavior. The parameters of the magnetosome-like response depend on aggregate state (suspension/pellet) of the cells, the "coercivity" of ReM_2 being larger/equal in response to suspensions for all the cell types. Subsequent experiments are necessary to elucidate the role of the iron-based magnetosome-like structures in the biology and physiology of the cells.

Higher concentrations of magnetosome-like structures followed by less "coercivity" of their $M_2(H)$ response are found in all mouse tissues (except for tumor) compared to rat tissues. Intriguingly, the magnetic parameters of magnetosome-like structures in well-oxygenated (brain, heart, lungs) mouse tissues correspond to single-domain magnetite nanoparticles in SPM regime with an average diameter of ~ 13 nm, whereas magnetosome-like structures of tumor and other organs with a

lower oxygen supply revealed hysteretic $M_2(H)$ signals more corresponding to Fe(0) multi-domain magnetic core.

Acknowledgements The authors thank Olga G. Genbach and Prof. Oleg V. Galibin for assistance in animal experiments and Ivan I. Larionov for assistance in NLR-M_2 measurements.

Funding This work was supported by the Alexander von Humboldt fellowship, by the DFG grant SFB824, by the Russian Foundation for Basic Research 19-08-00024; Technische Universität München (TUM) within the DFG funding programme Open Access Publishing; British Council Institutional Links grant, ID 277386067, under the Russia-UK partnership.

Compliance with ethical standards

Conflict of interest The authors declare no competing financial interests.

References

1. D.A. Bazylinski, R.B. Frankel, Nat. Rev. Microbiol. **2**, 217–230 (2004)
2. R. Blakemore, Science **190**, 377–379 (1975)
3. Y.A. Gorby, T.J. Beveridge, R.P. Blakemore, J. Bacteriol. **170**, 834–841 (1988)
4. K. Grünberg, E.C. Müller, A. Otto, R. Reszka, D. Linder, M. Kube, R. Reinhardt, D. Schüler, Appl. Environ. Microbiol. **70**, 1040–1050 (2004)
5. R.B. Frankel, D.A. Bazylinski, M.S. Johnson, B.L. Taylor, Biophys. J. **73**, 994–1000 (1997)
6. S. Bellini, Chin. J. Oceanol. Limnol. **27**, 6–12 (2009)
7. C.T. Lefèvre, L.F. Wu, Trends Microbiol. **21**, 534–543 (2013)
8. C. Jogler, D. Schüler, Annu. Rev. Microbiol. **63**, 501–521 (2009)
9. S. Baek, X. Quan, S. Kim, C. Lengner, J.K. Park, J. Kim, ACS Nano **8**, 10125–10138 (2014)
10. M. Pesce, A. Patruno, L. Speranza, M. Reale, Eur. Cytokine Netw. **24**, 1–10 (2013)
11. J. Yan, L. Dong, B. Zhang, N. Qi, Electromagn. Biol. Med. **29**, 165–176 (2010)
12. K.S. Kang, J.M. Hong, J.A. Kang, J.W. Rhie, Y.H. Jeong, D.W. Cho, Exp. Mol. Med. **45**, e6 (2013)
13. R. Gaetani, M. Ledda, L. Barile, I. Chimenti, F. De Carlo, E. Forte, V. Ionta, L. Giuliani, E. D'Emilia, G. Frati, F. Miraldi, D. Pozzi, E. Messina, S. Grimaldi, A. Giacomello, A. Lisi, Cardiovasc. Res. **82**, 411–420 (2009)
14. K. Maeda, K.B. Henbest, F. Cintolesi, I. Kuprov, C.T. Rodgers, P.A. Liddell, D. Gust, C.R. Timmel, P.J. Hore, Nature **453**, 387–390 (2008)
15. J.L. Kirschvink, M.M. Walker, C.E. Diebel, Curr. Opin. Neurobiol. **11**, 462–467 (2001)
16. M.A. Shevtsov, B.P. Nikolaev, V.A. Ryzhov, L.Y. Yakovleva, Y.Y. Marchenko, M.A. Parr, V.I. Rolich, A.L. Mikhrina, A.V. Dobrodumov, E. Pitkin, G. Multhoff, Nanoscale **7**, 20652–20664 (2015)
17. M.A. Shevtsov, M.A. Parr, V.A. Ryzhov, E.G. Zemtsova, A.Y. Arbenin, A.N. Ponomareva, V.M. Smirnov, G. Multhoff, Sci. Rep. **6**, 29247 (2016)
18. M.A. Shevtsov, B.P. Nikolaev, V.A. Ryzhov, L.Yu. Yakovleva, A.V. Dobrodumov, Y.Y. Marchenko, B.A. Margulis, E. Pitkin, A.L. Mikhrina, I.V. Guzhova, G. Multhoff, Nanomed. Nanotechnol. Biol. Med. **12**, 611–621 (2016)
19. V. A. Ryzhov, E. I. Zavatskii. Patent No 2507525, registered in Russia 20.02.2014
20. G.K. Anisimov, R.P. Devyaterikov, E.I. Zavatskii, V.V. Lavrov, V.A. Ryzhov, D.M. Fel'dman, V.N. Fomichev, Sov. Phys. Tech. Phys. **27**, 46–50 (1982)
21. V.A. Ryzhov, I.I. Larionov, V.N. Fomichev, Tech. Phys. **41**, 620–626 (1996)

22. P.V. Kharitonskii, K.G. Gareev, S.A. Ionin, V.A. Ryzhov, Yu.V Bogachev, B.D. Klimenkov, I.E. Kononova, V.A. Moshnikov, J. Magn. **20**, 221–228 (2015)
23. A.V. Lazuta, V.A. Ryzhov, V.V. Runov, V.P. Khavronin, V.V. Deriglazov, Phys. Rev. B. **92**, 14404–14411 (2015)
24. V.A. Ryzhov, I.V. Pleshakov, A.A. Nechitailov, N.V. Glebova, E.N. Pyatyshev, A.V. Malkova, I.A. Kiselev, V.V. Matveev, Appl. Magn. Reson. **45**, 339–352 (2014)
25. V.A. Ryzhov, A.V. Lashkul, V.V. Matveev, P.L. Molkanov, A.I. Kurbakov, I.A. Kiselev, K.G. Lisunov, D. Galimov, E. Lähderanta, JMMM **445**, 84 (2018)
26. S. Bedanta, W. Kleemann, J. Phys. D Appl. Phys. **42**, 013001 (2009)
27. F.F. Torres de Araujo, M.A. Pires, R.B. Frankel, C.E.M. Bicudo, Biophys. J. **50**, 375–378 (1986)
28. D.A. Bazylinski, D.R. Schlezinger, B.H. Howes, R.B. Frankel, S.S. Epstein, Chem. Geol. **169**, 319–328 (2000)
29. P.A. Guimaraes, *Principles of Nanomagnetism* (Springer, Berlin, 2009), p. 38
30. F.F. Guo, W. Yang, W. Jiang, S. Geng, T. Peng, J.L. Li, Environ. Microbiol. **14**, 1722–1729 (2012)

Affiliations

Vyacheslav A. Ryzhov[1] · Gabriele Multhoff[2] · Maxim A. Shevtsov[2,3,4,5]

Vyacheslav A. Ryzhov
ryzhov@omrb.pnpi.spb.ru

1 NRC "Kurchatov Institute", Petersburg Nuclear Physics Institute, Gatchina 188300, Russia

2 Klinikum rechts der Isar, Radiation Immuno-Oncology Group, Center for Translational Cancer Research Technische Universität München (TranslaTUM), Einsteinstr. 25, 81675 Munich, Germany

3 Institute of Cytology, Russian Academy of Sciences (RAS), Tikhoretsky Ave., 4, St. Petersburg 194064, Russia

4 First Pavlov State Medical University of St. Petersburg, L'va Tolstogo Str. 6/8, St. Petersburg 197022, Russia

5 Almazov National Medical Research Centre, Russian Polenov Neurosurgical Institute, Mayakovskogo Str. 12, St. Petersburg 191104, Russia